Key Points:

- First simultaneous observations of magnetically conjugate SAR arcs show a brighter arc in the Southern Hemisphere
- Seasonal variations in SAR arc brightness are caused by different local background ionospheric conditions
- Similar changes in brightness and motion of SAR arcs occur in both hemispheres and are related to changes in magnetospheric forcing

Supporting Information:

- Supporting Information S1
- Movie S1
- Movie S2

First Ground-Based Conjugate Observations of Stable Auroral Red (SAR) Arcs

C. Martinis[1] ![ID], J. Baumgardner[1], M. Mendillo[1], M.J. Taylor[2] ![ID], T. Moffat-Griffin[3] ![ID], J. Wroten[1] ![ID], C. Sullivan[1], R. Macinnis[1], B. Alford[1], and Y. Nishimura[1] ![ID]

[1]Center for Space Physics, Boston University, Boston, MA, USA, [2]Center for Atmospheric and Space Sciences and Physics Department, Utah State University, Logan, UT, USA, [3]British Antarctic Survey, Cambridge, UK

Abstract During the geomagnetic storm of 1 June 2013, all-sky imagers located at geomagnetically conjugate locations at Millstone Hill, USA (42.6°N, 71.4°W, 50.9° mag lat) and at Rothera, Antarctica (67.5°S, 68.1°W, -53.2° mag lat), allowed us to measure a stable auroral red (SAR) arc simultaneously in both hemispheres for the first time. The arc measured in one hemisphere was observed very close to its conjugate location in the opposite hemisphere. While spatial characteristics, such as equatorward motion and latitudinal extent, were similar at both sites, morphological properties, for example, arc brightness and shape of the poleward edges, differed. The overall brightness of the northern hemisphere arc was considerably weaker, by a factor of ~2-3, throughout the night. Reduced magnetospheric forcing, in a short time interval between ~0345 UT and 0445 UT, led to decreased SAR arc brightness and reduced equatorward motion at both sites. A substorm occurring near 0500UT provided additional energization that increased the SAR arc brightness as well as the speed of the equatorward motion. These results provide evidence of a complex coupling between energy sources in the inner magnetosphere and the ionospheric receptor conditions within the subauroral domain at opposite ends of the same geomagnetic field line.

1. Introduction

1.1. MI Coupling at Subauroral Latitudes

Magnetosphere-ionosphere (MI) coupling has long been studied in the polar and auroral regions where most of the interaction occurs. At lower latitudes, that is, equatorward of the diffuse aurora, the subauroral ionosphere offers an additional example of MI coupling, in this case with the inner magnetosphere. One of the consequences of this coupling is the occurrence of optical emissions at 630.0 nm produced by the transition of an oxygen atom from its excited (^{1}D) state to the ground energy state. The phenomenon is known as a stable auroral red (SAR) arc (Barbier, 1960). SAR arcs have distinct characteristics (narrow in latitude, broad in longitude) that have been described using wide field imagers from single-site ground-based observatories (Slater et al., 1986; Mendillo et al., 1987; Mendillo et al., 2016) and from satellite measurements (Craven et al., 1982). During periods of high geomagnetic activity, SAR arc features, usually constrained to ~60-65° magnetic latitude, are enhanced and their spatial extent reaches lower latitudes (50°–55°). Figure 1 shows a schematic of the inner magnetosphere with two rings labeled 'conjugate sar arcs' that represent the ionospheric foot-points of the overlapping plasmasphere and ring current regions. SAR arcs are found at the equatorward edge of this boundary. They are typically ~500 Rayleighs (R) in brightness—about 10 times fainter than visible faintest red aurora (Chamberlain, 1995). The excitation of the O^{1}D state requires ~2eV, and this is provided by collisions between ambient O atoms and ionospheric electrons that have been heated to T_e > 3,000 K by heat flux from the ring current. Yet such electron-oxygen collisions do not produce emissions at 557.7 nm from the O^{1}S state (~5 eV), and thus, SAR arcs are spectrally pure 'red line' features. Comprehensive reviews of SAR arc formation and morphologies are given in Rees and Roble (1975), Kozyra et al. (1997), and Baumgardner et al. (2013).

1.2. Single Hemisphere Site Measurements

Most SAR arcs have been observed in the northern hemisphere, and from North America in particular (e.g., Slater & Smith, 1981; Mendillo et al., 2016). Yet there are a few reports from the southern hemisphere, for example, in South Africa by Carman et al. (1973), in Australia by Schaeffer and Jacka (1971) and Glass et al. (1970), and in New Zealand by Mendillo et al. (2013). During the large geomagnetic storm of 17-18
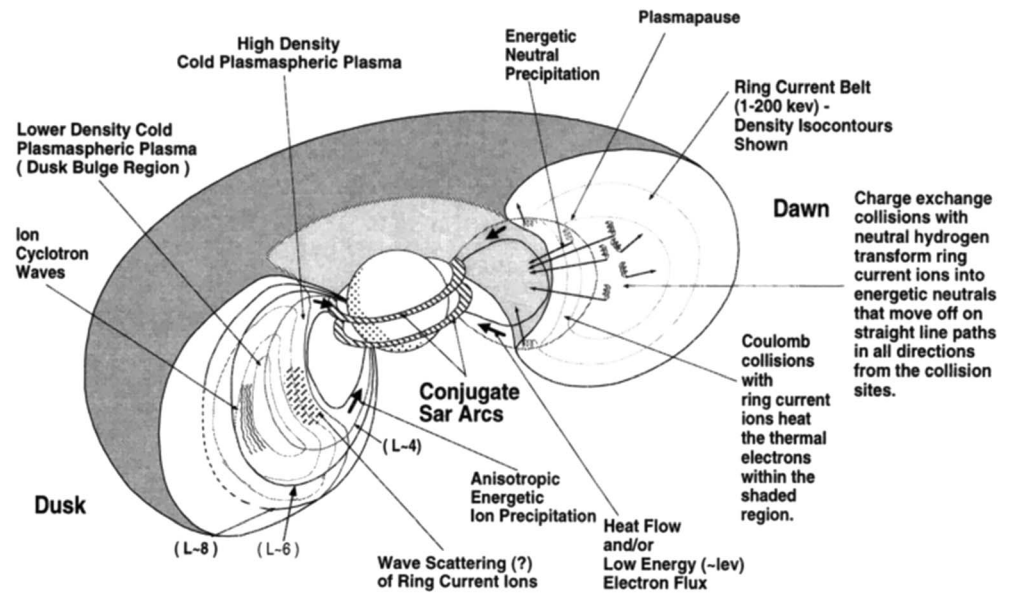
Figure 1. Schematic representation of the inner magnetosphere showing the overlap between the ring current and plasmasphere. The resultant toroidal ring extends around the Earth. Stable auroral red arc emissions occur at the foot of field lines that thread this overlapping region. Ring current loss processes are summarized. (from Kozyra et al., 1997).

December 1971, Carman et al. (1973) observed unusual emissions at 630.0 nm reaching ~200 R looking toward the south at ~45° geomagnetic invariant latitude. With no accompanying 557.7-nm emission, the feature was interpreted as a SAR arc. The study by Schaeffer and Jacka (1971) included red line and green line photometers. Their observations of the red line indicated an equatorward motion during a storm. The green line distribution did not match the red line data and was found to be produced by a different source, verifying the monochromaticity of the SAR arc. Airborne observations were carried out over Australia by Glass et al. (1970), who described a single SAR arc event on 15 May 1969 and discussed its equatorward propagation and alignment with constant L-shell curves (L-shell is a parameter defined as the distance in Earth radii of a magnetic field line crossing the magnetic equator). More recently, Mendillo et al. (2013) demonstrated the large temporal coverage of SAR arcs using two all-sky imagers (ASIs) in the northern hemisphere and one in the southern hemisphere. The study showed for the first time the occurrence of an arc during 24 consecutive hours.

1.3. Past Conjugate Observations

Conjugate observations of SAR arcs using satellite data have been reported by Reed and Blamont (1974) and LaValle and Elliott (1972). The Reed and Blamonts study was a brief report on the SAR arc of 28-30 September 1967 observed by the photometer onboard the Ogo-4 spacecraft. It was compared with photometer results from one ground station in Idaho, North America (Ichikawa et al., 1969), and the peak brightness levels were in excellent agreement (230 R from the ground and 185 R from Ogo-4). The Ogo-4 data in the southern hemisphere located the SAR arc within a few tenths of the L-value recorded in Idaho (L ~3). Yet the brightness determined by the satellite in the northern hemisphere was about 60% greater than the value observed in the southern hemisphere. LaValle and Elliott (1972) analyzed three SAR arcs from the satellite OV1-10 that was launched in 1966 into a polar orbit. One of the SAR arcs was observed as a conjugate phenomenon on 16 February 1967. Brightness values did not differ much in both hemispheres: 510 R in the northern hemisphere as compared with 645 R in the southern hemisphere. These two studies indicate that interhemispheric differences in brightness were larger in equinox and very small during January solstice. Ground-based studies in both hemispheres were presented by Roach and Roach (1963). They reported SAR arc observations in North America and in New Zealand, but at different times, that is, not simultaneous conjugate observations were performed.
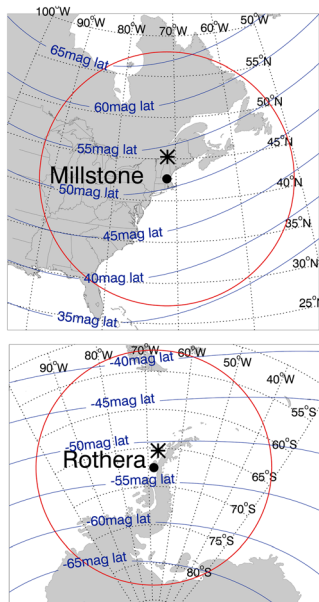
Figure 2. (top) Field-of-view of the Millstone Hill all-sky imager for zenith angles <85° and emission height at 400 km; (bottom) field-of-view of Rothera's all-sky imager. The solid black circles refer to zenith at each location, and the asterisks represent their geomagnetic conjugate points.

Seasonal studies have been described by several groups using ground-based data only from a northern hemisphere site (Fok et al., 1993; Kozyra et al., 1997). The seasonal patterns they addressed had to be acquired sequentially and therefore during different geomagnetic storms. Their statistical findings were that emission levels were lowest in summer months. The two conjugate observations from satellite data described above are not consistent with these statistical results. Thus, previous data sets available to assess seasonal and/or conjugate point differences are not yet conclusive.

There are no reports in the published literature of simultaneous observations of SAR arcs from conjugate ground-based locations. SAR arc studies using two ground-based data sets linked by the same geomagnetic field line, that is, *conjugate-point studies*, allow seasonal patterns and other hemispheric characteristics to be obtained *simultaneously*, not sequentially, as presented above. The two stations used in this study, Millstone Hill (USA) and Rothera (Antarctica), have different geographic latitudes (42.6°N versus 67.5°S) but similar magnetic latitudes (50.9° mag lat N versus 53.2° mag lat S). Spring and fall SAR arcs can be observed simultaneously since the duration of night is approximately the same at both stations. Winter and summer events, however, can only be obtained simultaneously during the months spanning the June solstice: summer at Millstone Hill and winter at Rothera. No simultaneous observations are possible in December since "midnight sun" conditions occur in Rothera.

Previous works addressing 'seasonal asymmetries' relied on measurements at a single site during different seasons, implying different underlying thermosphere-ionosphere or background, conditions, and different storm conditions. In this work we show for the first time simultaneous interhemispheric characteristics of SAR arcs using ASIs in North America and Antarctica during the 1 June 2013 storm. The possibility of measuring simultaneously in both hemispheres will allow us to assess if any asymmetries observed are due to local 'receptor' (i.e., seasonal) ionospheric background conditions or to intrinsic M-I coupling differences.

2. Observations

The SAR arc observations used in this study come from ASIs that are components of the Boston University all-sky imaging network (Martinis et al., 2017) located at Millstone Hill Haystack Observatory and at Rothera Research Station, sites geomagnetically conjugate to each other. Figure 2 shows the field-of-view (FOV) of the ASIs located at Millstone Hill (top) and Rothera (bottom). The FOVs are computed for an emission height of 400 km, appropriate for SAR arcs (Tohmatsu & Roach, 1962). The asterisk in each map represents the geomagnetically conjugate point of the zenith location of the ASI in the opposite hemisphere. The IGRF-12 model (Thébault et al., 2015) was used to compute conjugate locations, and quasi-dipolar coordinates (Richmond, 1995) were used to draw lines of constant magnetic latitude. The Millstone ASI currently uses a $1{,}024 \times 1{,}024$ back-illuminated charge-coupled device camera with small readout noise (~3 el RMS). A filter wheel houses five interference filters used to measure different mesospheric and thermospheric emissions, as well as off-band (background) scattered light. For this study we use images that were binned 2×2, taken at 630.0 nm every 8 min with an exposure time of 120 s.

Observations in 630.0-nm emission at Rothera started in 2011 as part of a collaborative observational project between Boston University's Center for Space Physics, the Center for Atmospheric and Space Science at Utah State University, and the British Antarctic Survey. Rothera (67.5°S, 68.1°W) is located on Adelaide Island to the west of the Antarctica Peninsula. The Rothera ASI is a multifilter system, with five different filters and is typically used to study mesospheric gravity waves as part of the international Antarctic Gravity Wave Instrument Network (ANGWIN). Rothera data are also binned down to 512×512, and 630.0-nm images are taken with a 90-s exposure every seven and a half minutes. Nighttime measurements
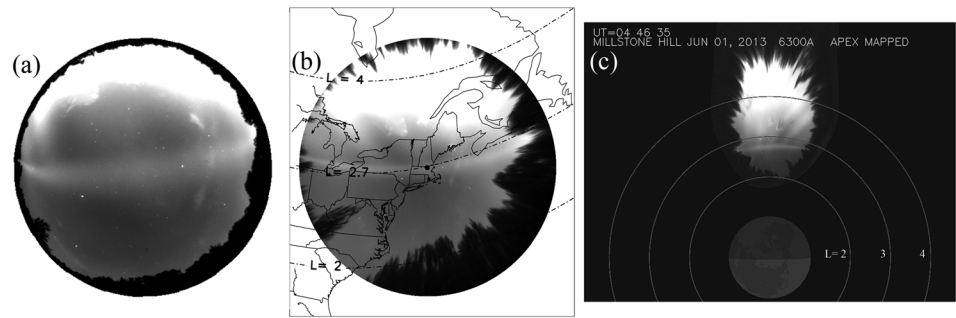
Figure 3. All-sky image in 630.0 nm that shows a stable auroral red arc and the diffuse aurora in (a) raw data format and (b) "unwarped" upon a geographic map for an assumed emission altitude of 400 km. Trees at low-elevation angles restrict useable data to ~160° field of view. Lines with constant L-shell values are shown for L=2, L=2.7, and L=4; (c) mapped into the geomagnetic equatorial plane. L values of 2, 3, and 4 are shown.

are limited to the period between March and October, with the rest of the year unavailable due to summer time 'white nights'.

The availability of 630.0-nm data at these two sites offers the opportunity to investigate the interplay between ambient ionospheric conditions (ordered by geographic latitude) and storm time coupling processes (ordered by geomagnetic latitude) that, collectively, contribute to the optical manifestation of M-I coupling in the subauroral domain. Previous studies of SAR arcs using photometers in the northern hemisphere (Slater & Smith, 1981) revealed a semiannual pattern with peaks roughly during equinox months and minimum during the July solstice period. This is important for the Millstone Hill-Rothera pair of stations because Rothera's high geographic latitude (67.5°S) has months of continuous sunlight when ASI data cannot be taken (from mid-October to mid-March). Weather conditions show on average 40% clear nights at Rothera during the observing season, with winter months having most of the clear nights. Imaging data at Millstone Hill are taken every month of the year (with local summer months having shorter nighttime periods of operation).

3. SAR Arc Characteristics

The SAR arcs described in this study occurred simultaneously during a moderate geomagnetic storm on 1 June 2013 with Dst peaking at only -137 nT. Nevertheless, extreme effects were reported at midlatitudes by Martinis et al. (2015). Different aspects related to magnetospheric processes during this storm were also studied, including O^+ ion conic dynamics (Burke et al., 2016), the role of large-scale duskward electric fields in ring current formation and plasmasphere erosion (Thaller et al., 2015), and the source of O^+ in the ring current (Kistler et al., 2016). Here we investigate the storm effects at subauroral latitudes.

With instrumentation at Millstone Hill and Rothera, we now have the possibility of measuring simultaneously for the first time how the location and brightness of the arcs compare at both hemispheres.

3.1. Location

A SAR arc does not occur in a thin emission layer, but rather has a centroid of emission spanning the 350- to 450-km altitude domain (Roach & Roach, 1963). Throughout this study, we used processed images that were unwarped to a height of 400 km. There is an uncertainty in the unwarped location of a pixel due to the emission height assumed. For the location of the SAR arcs spanning zenith angles less than 60° this is insignificant. For example, for a pixel at 30° zenith angle a change in altitude of ±50 km produces a shift of $\pm$ 0.2° in latitude and $\pm$ 0.06° in longitude. Figure 3a shows a Millstone Hill raw all-sky image in 630.0 nm with the diffuse aurora at the top (north) and a weaker east-west extended SAR arc closer to zenith. Panel (b) shows the same image unwarped into a latitude and longitude map assuming a height of 400 km. L-shell values are shown as solid lines. Panel (c) shows the same image now mapped into the equatorial plan where the arc is seen to occur below L=3; this representation is useful when trying to find conjunctions with satellites measuring magnetospheric properties, like the THEMIS (Time History of Events and Macroscale Interactions during Substorms) mission or the VAP (Van Allen Probe) mission.

01 June 2013
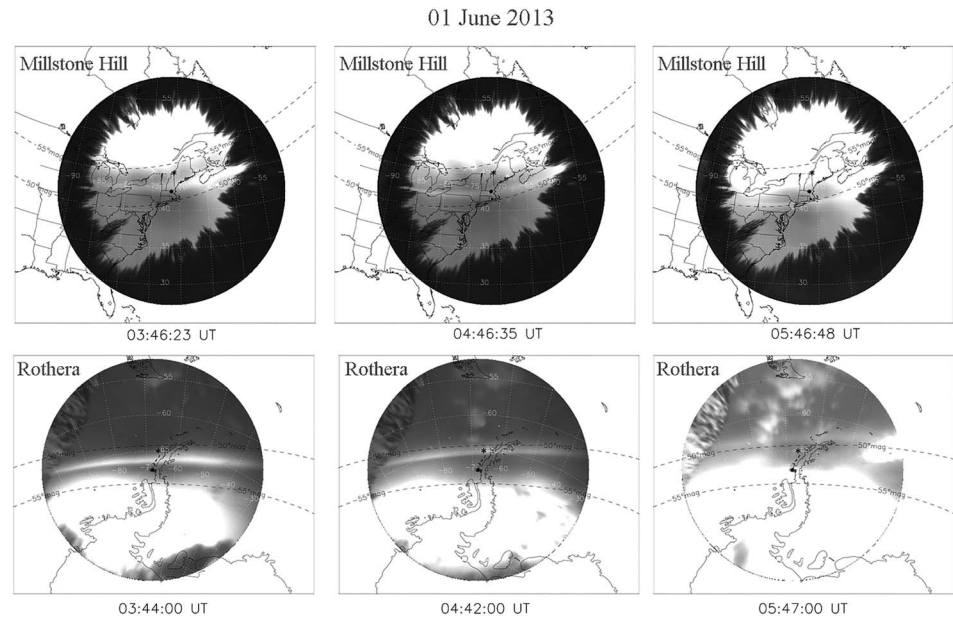
Figure 4. Simultaneous images from (top) Millstone Hill ASI and (bottom) Rothera ASI at three different times: (left) ~0345 UT, (center) ~0445 UT, and (right) ~0546 UT. The black circles indicate the zenith location of the imagers, and the asterisks show their respective conjugate points. Magnetic latitude lines at $\pm 50°$ and $\pm 55°$ are also shown.

Figure 4 shows uncalibrated unwarped all-sky images at Millstone Hill (top) and the corresponding Rothera images (bottom). The circle in each image represents the zenith location, and the asterisk indicates the conjugate location of the imager in the opposite hemisphere. Movies from both sites are included as supporting
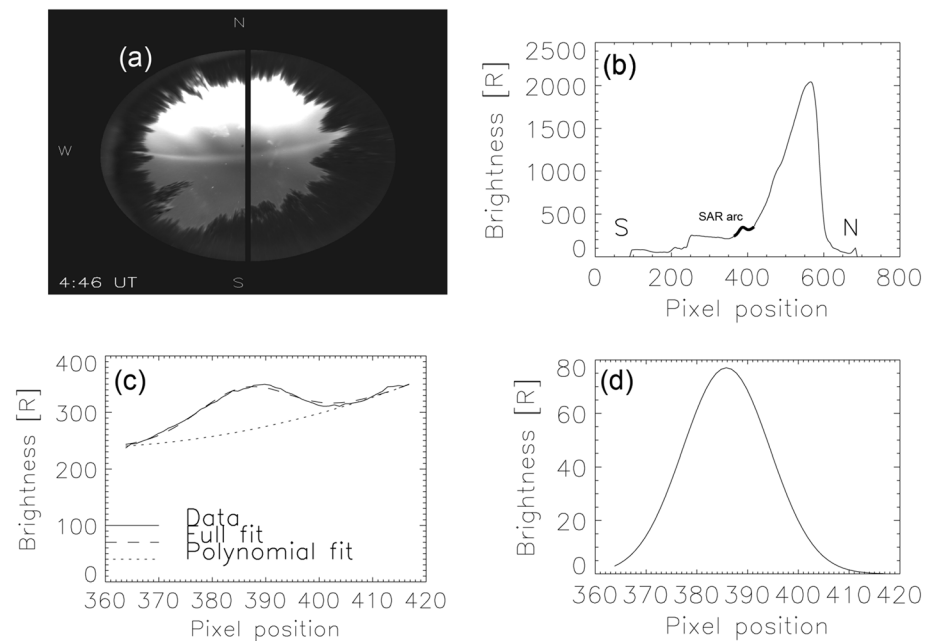
Figure 5. (a) Unwarped and calibrated Millstone Hill image at 0446UT. The black line represents a north-south 10-pixel-wide meridian cut. (b) Average cut covering the entire image. The pixel positions in the horizontal axis can be uniquely related to geographic latitudes. The thick superposed curve represents the subrange of data that will be fitted to obtain stable auroral red arc parameters. (c) Stable auroral red arc data obtained from the average cut (solid line), full fit (dashed line), and polynomial fit (dotted line). (d) Resulting Gaussian fit obtained by subtracting the full and polynomial fits shown to the left. From this curve the brightness, location, and width of the arc can be obtained.
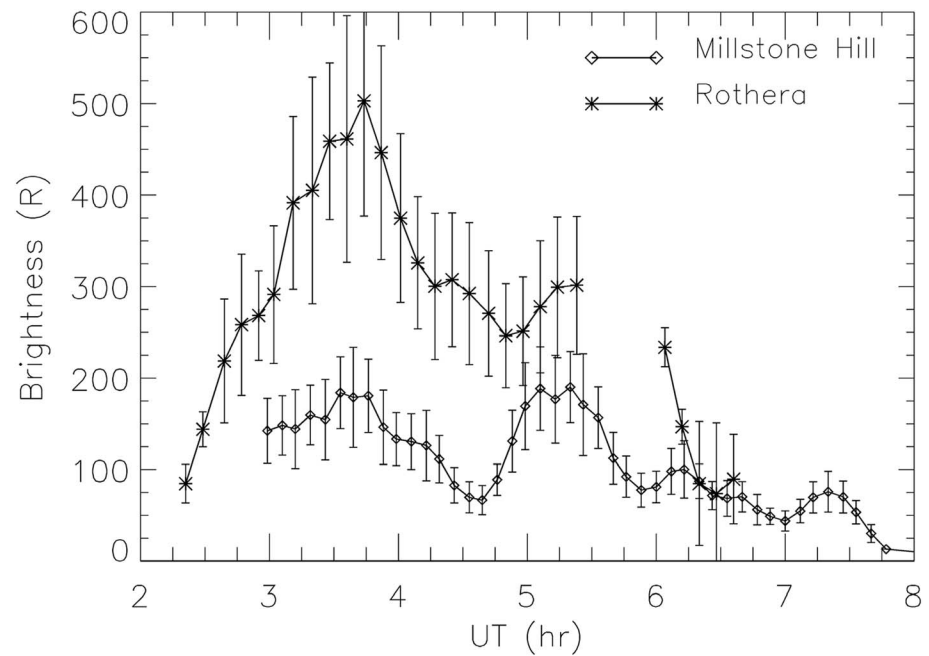
Figure 6. Millstone Hill (diamonds) and Rothera (asterisks) stable auroral red arc brightness. The stable auroral red arc curves at both sites follow a similar trend, with Rothera being larger than Millstone Hill. The error bars represent the uncertainty in the determination of the brightness values. The small gap in the Rothera curve is due to clouds that affected the fitting process.

information. The three panels in Figure 4 show simultaneous images taken at ~0345, 0445, and 0545 UT. The saturated features to the north of Millstone Hill and south of Rothera images represent bright diffuse aurora. The arcs are observed at the same magnetic latitudes in both hemispheres; that is, they are magnetically conjugate. The middle panel shows the arc overhead at Millstone Hill, and the arc observed at Rothera falls right on top of the conjugate location of Millstone Hill. Both arcs seem to have similar width, although one of the main differences observed is that the poleward edge of the arc at Rothera is sharper and less diffuse than the one observed at Millstone Hill. A quantitative comparison of brightness and edges of the arcs is discussed below.

3.2. Brightness

Central to this study is the issue of brightness calibration. In order to do this we need to use calibrated images with brightness expressed in units of Rayleighs. The two ASIs use cameras and optics with different characteristics. For this study both systems were calibrated using visible stars (Martinis et al., 2013). The Millstone Hill system also has the capability of calibration using a standard C-14 source (Baumgardner et al., 2007). For consistency, the calibration using stars was compared with the procedure using a C-14 source. This allowed for validation using two methods at Millstone Hill, and if atmospheric scattering corrections were included, results showed good agreement. The resulting two-site calibration method using stars give image brightness levels expressed in Rayleigh units, with an uncertainty of ±25%, arising collectively from systematic errors in the calibration process, error uncertainty from the fitting procedure, and more importantly, uncertainty due to atmospheric scattering.

We describe the method employed to extract the key parameter of SAR arc brightness (in Rayleighs, R) *above* background levels. This is the emission driven by external sources, independent of all forms of local airglow levels and scattered light. An example of the image processing method for determining SAR arc characteristics is shown in Figure 5. A 10-pixel-wide north-south cut is taken along the central meridian of each image, as shown in panel (a). Pixel location in the north-south direction increases from the bottom of the figure. The meridional cut is averaged, and the resulting curve is shown in panel (b). The horizontal axis in pixel values is uniquely related to geographic latitude, so increasing pixel values represent increasing latitudes. Background airglow is observed until pixel position 300; the small bump between pixel positions ~300
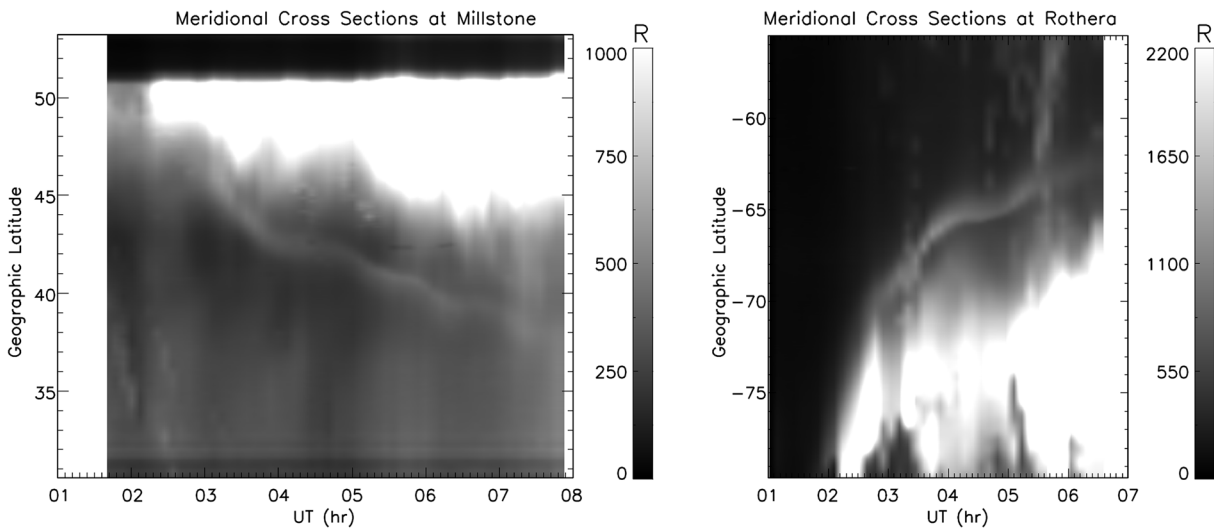
Figure 7. (left) Meridional cuts 10-pixel-wide from Millstone Hill. The bright structures on the top are auroral signatures. The stable auroral red arc appears around 0300 UT at ~47° geographic latitude. (right) Meridional cuts 10-pixel-wide from Rothera. The stable auroral red arc is observed before 0300 UT.

and ~500 is the SAR arc; the higher values after pixel position 500 are the bright emissions from the diffuse aurora. We select a segment of the entire curve that includes the left and right flanks of the bump that reflects the SAR arc structure. A function including a second-order polynomial and a Gaussian curve is used to fit this segment of data, as indicated in panel (c). Quantitative SAR arc characteristics can be obtained from the fitted Gaussian curve. We are interested in three main SAR arc characteristics that can be related to parameters obtained from the fitted curve: brightness (amplitude), location (center), and latitudinal extent (width). The combined non-Gaussian terms (i.e., constant, first- and second-order polynomials) are shown as the dashed line in panel (c). In the same plot the segment of interest data is shown as a solid curve and the Gaussian as a dotted curve. The final result in panel (d) is the detrended Gaussian fit obtained by subtracting the full and polynomial fits shown in panel (c). From this final curve the brightness, location, and width of the SAR arc are obtained. The brightness of the SAR arc is obtained from the amplitude of the curve shown in panel (d), and it represents the background subtracted brightness

Figure 6 shows the resulting brightness values (background subtracted) for the SAR arcs at Millstone Hill and Rothera for all the images taken on 1 June 2013. The ~30-min data gap in the Rothera curve represents a brief period when clouds affected the calibration at this site. A $\pm 25\%$ uncertainty in brightness is shown in each data point. The SAR arc at Rothera is brighter than the one observed at Millstone Hill, by a factor of 2-3. Both arcs increase in brightness until ~0330UT. Interestingly, there is a decrease in the brightness at both sites between 0345 and 0445 UT, with Rothera going from ~450 to ~300 R and Millstone Hill from ~200 to 75 R. This decrease is followed by a brightening of both arcs until ~0545UT. As we will discuss later this is related to changes in solar wind/magnetospheric activity, as measured by different solar wind parameters, geomagnetic indices, and particle flux data.

3.3. Meridional Motion

In addition to the variations in brightness observed, the full set of conjugate images can be used to investigate the meridional motion of the SAR arcs. The arcs move equatorward in response to natural local time variation of the plasmapause/ionospheric trough location and to enhanced magnetospheric activity. The possibility of measuring simultaneously the dynamics of SAR arcs in both hemispheres provides a new tool to investigate how these ionospheric manifestations of the plasmapause-ring current inner boundary respond to forcing from solar wind-magnetosphere drivers.

In order to compare the equatorward motion of the arcs their velocities were computed by creating meridional cuts, 10 pixel wide, from which velocities were determined. Figure 7 (left) shows the result for Millstone Hill. The bright saturated regions to the north represent the diffuse aurora. The SAR arc is identified by the descending curve with a large bump around 0400UT and smaller ones at ~0600 UT and ~0700 UT. An identical analysis for Rothera is shown to the right. The arc is distinguishable earlier, at around 0230UT, very
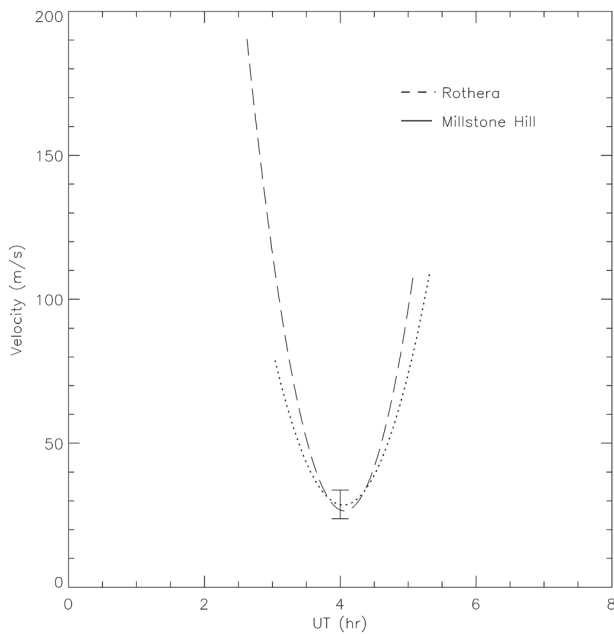
Figure 8. Stable auroral red arc velocity obtained from the velograms in Figure 7. Both curves show similar behavior, with decreasing speeds until ~0400 UT. After this time the arcs move with increasing speeds. A 10-m/s error bar is drawn at 0400UT.

close to the equatorward boundary of the diffuse aurora. The main bump around 0400UT is also seen here. Clouds made it difficult fitting the arc observations between ~0530UT and 0600 UT. In order to compare the motion of the SAR arc at both sites, and since Rothera data are available only until 0700UT, a third-order polynomial was fit to the latitudinal position from ~0300UT to 0600UT. The velocity is obtained by taking the derivative of the fitted curve. The result, shown in Figure 8, indicates that both arcs seem to be moving initially at similar decreasing velocity, with the Rothera arc velocity slightly larger, going through a minimum at around 0400 UT, and speeding up later, again with the Rothera arc moving faster. The error in the determination of the velocity is ± 5 m/s, making difficult to conclude that in fact the Rothera arc moves faster. The movies in the supporting information show how the equatorward motion of the arcs changes during the night, verifying the results shown in Figure 8; that is, both sites show that the arcs motion is not uniform during the night, with a brief period of time when the propagation speed goes through a minimum. This behavior is likely related to forcing mechanisms that affect how rapidly the inner boundary of the ring current moves earthward during the nighttime.

3.4. Latitudinal Shape

Another striking difference between the conjugate SAR arcs appears when the meridional shapes of the arcs are compared. Figure 9 shows SAR arc data for three different times: 0345, 0445, and 0545UT, corresponding to the images shown in Figure 4, and the corresponding fitted curves, as described earlier, but now with the horizontal axis representing geographic latitude (there is a direct relationship between pixels and geographic latitude). The left plots show the results for Millstone Hill images, and the plots to the right show the simultaneous Rothera images. Both SAR arcs have similar
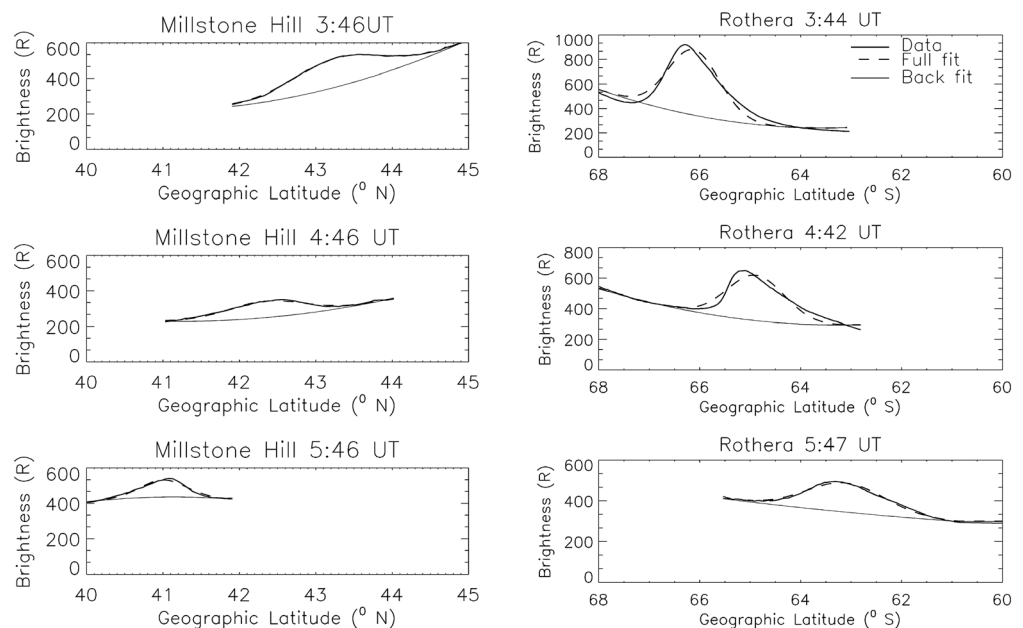
Figure 9. (left) Meridional cut showing symmetric shapes at Millstone Hill at three different times: (top) 0345 UT, (middle) 0445 UT, and (bottom) 0545 UT. (right) Similar plots for the stable auroral red arc over Rothera. Stable auroral red arc shapes at Rothera show stronger gradients at higher latitudes, that is, at the poleward boundary.
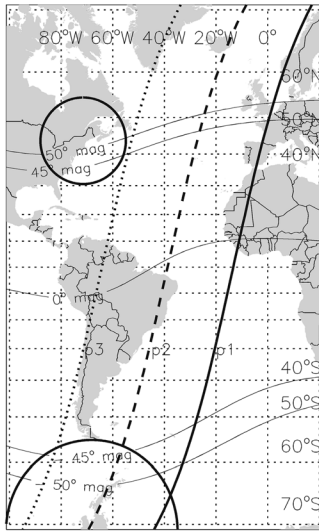
Figure 10. Defense Meteorological Satellite Program (DMSP) F15 passes on 1 June 2013. The first pass (p1, thick solid line) crossed 50° mag latitude at 0° longitude at 0400UT; the second pass (p2,dashed thick line) at ~25°W at 0600UT; the third pass (p3,dotted line) at ~55°W at 0730UT. Circles represent 160° field-of-view of the all-sky imagers. Map is shown using a Mercator projection. Stable auroral red arc signatures are observed inside 45–50° and -45–50° magnetic latitudes.

widths (full-width at half-maximum), around 1.1°. Millstone Hill arcs present smooth symmetric shapes the entire night, but the arcs observed at Rothera show sharper poleward edges. Between ~0345 and ~0500 UT, this asymmetric shape seems to be more pronounced (see images at 0345 and 04:45 UT).

From the results described above we can state the following:

1. The SAR arc observed at one site is seen at its magnetically conjugate location.
2. The SAR arc at Rothera (winter) is brighter than the one observed at Millstone Hill (summer), by a factor of 2-3. Similar changes in brightness are observed at both sites throughout the night.
3. Both arcs show similar equatorward motion.
4. Both arcs have the same latitudinal width, around 1.1°, although the poleward edges of the arcs at Rothera are sharper.

4. Discussion

Past single hemisphere observations of SAR arcs have provided valuable information on their brightness characteristics and variabilities with season and solar activity. In this study, for the first time, simultaneous interhemispheric, magnetically conjugate observations of SAR arcs are presented. These observations allow the direct interhemispheric comparison of SAR arc brightness values and morphology characteristics during the same storm, thereby presenting pure seasonal effects rather than their statistical representations obtained over a spectrum of geomagnetic disturbances.

4.1. Seasonal Variation in SAR Arc Brightness

The SAR arc at Rothera (winter) is two to three times brighter than the one at Millstone Hill (summer). This result illuminates the difference between past statistical studies at single sites when seasonal effects appear as small-magnitude average differences and the result shown here at two sites located in different hemispheres, with large-magnitude differences observed. It is also in agreement with studies showing that SAR arc brightness reaches a minimum during local summer conditions (Fok et al., 1991; Slater & Kleckner, 1989). A brighter arc in the winter hemisphere could be explained by lower electron densities in the nighttime ionospheric F-layer (and its trough) that allow the energy generated in the inner magnetosphere to be distributed among fewer electrons, producing larger electron temperatures.

Defense Meteorological Satellite Program (DMSP) satellite data can be used to describe local ionospheric conditions in both hemispheres. Several passes of satellite F15 on 1 June 2013 showed signatures of SAR arcs, that is, enhanced T_e and decreased N_i (Baumgardner et al., 2013; Foster et al., 1994), at different longitudes. Figure 10 shows three DMSP 15 passes labeled P1, P2, and P3. The first pass in the northern hemisphere occurred at ~0400UT in the European sector. The last pass was closer to the field of view of the Millstone Hill ASI, around 0730 UT. The passes in the southern hemisphere go through longitudes being sampled by the Rothera ASI. Figure 11 shows DMSP ion densities and electron temperatures in the northern hemisphere (left) and in the southern hemisphere (right). Data from Pass 1 are shown in the top panel (a), and data from Pass 3 are shown in the bottom panel (b). Comparable magnetic latitudes (but not conjugate points) were sampled in these passes. In the northern hemisphere, the SAR arc signatures are detected in the first pass at ~50° magnetic latitude and 0° geographic longitude in the European sector, and in the southern hemisphere at ~45°W, inside the field of view of Rothera's ASI. The minimum N_i in the southern hemisphere is ~7×10³ e/cm³ and in the northern hemisphere is ~5×10⁴ e/cm³, almost an order of magnitude larger, a natural consequence of a stronger ionosphere due to local summer conditions. The corresponding T_e values increase from 3500 to ~5000 K in the northern hemisphere and from only ~2000 to ~6000 K in the southern hemisphere. Thus, we expect that the SAR arc in the northern hemisphere will be weaker than the one occurring in the southern hemisphere. Similar values are observed in Pass 3, with SAR arc signatures at ~45° magnetic latitude closer
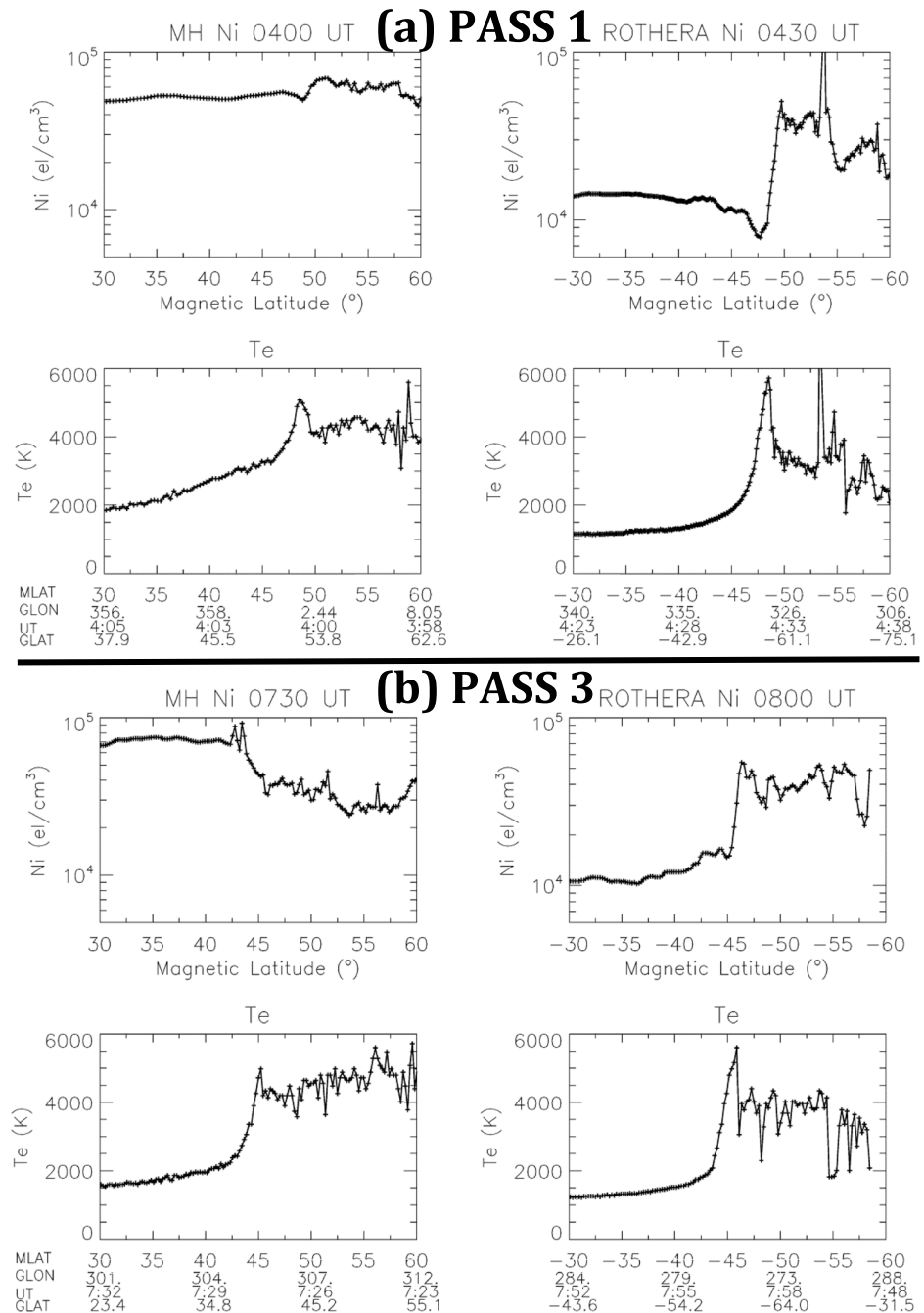
Figure 11. (a) PASS1: Defense Meteorological Satellite Program (DMSP) F15 observations of (top panels) total ion density N_i and (bottom panels) electron temperature T_e (left) in the northern hemisphere at ~ 0400UT and (right) in the southern hemisphere at ~0430UT. The typical signatures of a stable auroral red arc (low N_i, high T_e) are observed at subauroral magnetic latitudes ~50°, similar to the arcs locations. (b) PASS 3: similar to (a) but at 0730 UT in the northern hemisphere and ~0800 UT in the southern hemisphere. Stable auroral red arc signatures are observed at lower latitudes, around 45° magnetic latitude, in agreement with the all-sky imager observations at Millstone Hill (the Rothera all-sky imagers had stopped taking data at 0700UT).

to the FOV of the Millstone Hill ASI. The magnitude of the temperature enhancements and density reductions are very similar to those shown in Baumgardner et al. (2013) where a SAR arc of approximately few hundred Rayleigh was reported. Thus, the brighter arc observed at Rothera is consistent with this seasonal asymmetry in the background plasma density and temperature conditions.
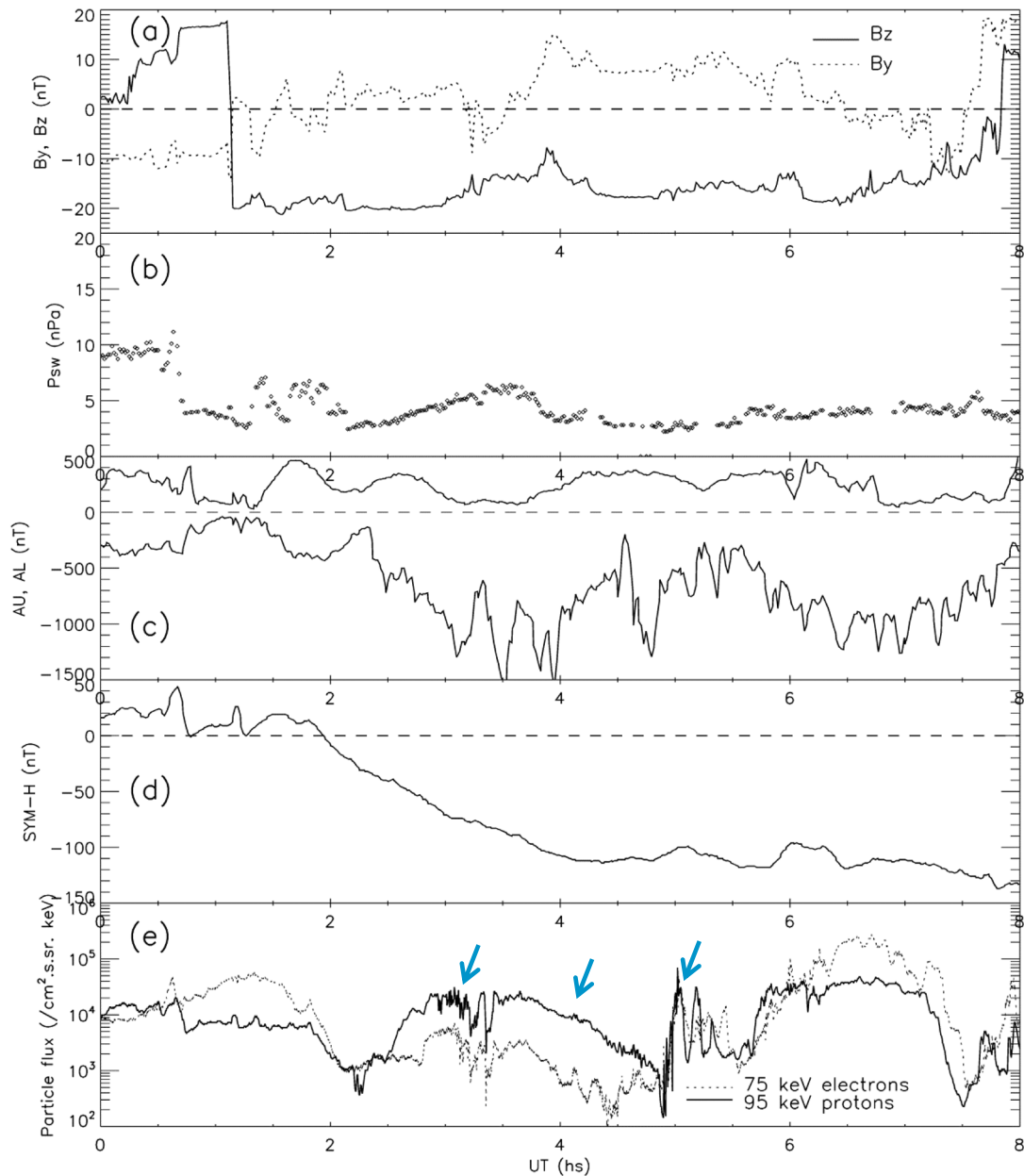
Figure 12. (a) Solar wind B_y and B_z components. (b) Solar wind pressure. (c) Auroral AU and AL indices. (d) Equatorial SYM-H index. (e) Particle flux from GOES-15. Arrows indicate the times when the brightness and speeds of the arcs change.

4.2. SAR Arc Characteristics

The discussion now will focus on the observation of three characteristics of the SAR arcs: equatorward motion, brightness variations, and latitudinal shape. The results show that both arcs move at similar velocity, going through a minimum at around 0400UT, with increasing velocity later. The fitted curves show that the arc at Rothera moves slightly faster than the one at Millstone Hill, but the uncertainty in the velocity determination makes it difficult to conclude that Rothera's arc moves faster. An important point to address for future inter-hemispheric comparisons is that in this longitude sector the south atlantic magnetic anomaly might be affecting the velocity in the southern hemisphere. The second characteristic is the brightness of the arcs and the fact that variations in their brightness are seen to occur simultaneously at both sites. Data show an overall increase in the brightness at both sites, followed by a decrease, with Rothera going from ~450 to ~300 R and Millstone Hill from ~200 to 75 R. These changes were followed by an increase in

brightness at both sites with Rothera reaching ~300 R and Millstone Hill ~200 R. Finally, the third characteristic is the latitudinal shape of the arcs. We find that they are different, with the Rothera arc showing a sharper poleward boundary, being more prominent between 0345 and 0500 UT.

The initial slowing down of the equatorward motion and decrease in brightness, followed by a faster equatorward motion and increase in brightness, can be related to magnetospheric forcing. Coulomb interactions between ring current ions and the thermal electrons in the outer plasmasphere are thought to be one of the main mechanisms by which energy can be transferred to the subauroral ionosphere (Kozyra et al., 1997). Therefore, we expect that the ring current evolution, related to solar wind-magnetospheric interactions, will affect the way the subauroral ionosphere receives the energy to trigger and maintain SAR arcs.

Figure 12 shows relevant solar wind parameters, geomagnetic indices, and particle fluxes for the period 0000UT to 0800UT on 1 June 2013: from top to bottom, (a) interplanetary magnetic field (IMF) components B_y and B_z; (b) dynamic pressure P_{sw}; (c) auroral electrojet indices, AU and AL; (d) equatorial SYM-H index, and (e) GOES-15 particle flux for 95-keV protons and 75-keV electrons. The main phase of the storm was triggered by the large IMF southward turning at ~0100UT, remaining strongly southward afterward. The blue arrows in panel (e) indicate the times when the brightness and speed of the arcs change. Clearly, they increased after 0200UT and decreased between ~0300 and 0345 UT. Particle injection occurred around ~0500UT (the satellite was at ~20 magnetic local time at 6.6 RE). There is an anticorrelation between the behavior of AL and SYM-H; this has been known to be caused by dipolarization in the inner magnetosphere followed by plasmoid ejection from the magnetotail (Noah & Burke, 2013), i.e., a substorm.

From these observations we can infer that initially the arcs increase their brightness until ~ 0345 due to enhanced magnetic activity (GOES-15, SYM-H, and AL are seen to increase). After this time, the IMF B_y turning from negative to positive and the reduction in the flow pressure most likely contributed to a reduction of the flow of earthbound particles, as seen by GOES-15. As a consequence, AL weakens to -400 nT and SYM-H remains constant. This contributed to produce dimmer arcs, as well as a decrease in their equatorward motion. Around ~0500UT, when additional energization occurs (GOES-15 detected particle injection and dipolarization due to the ~0440 UT substorm, so AL increased), both arcs are brighter and move at an increasing speed. This supports the interpretation that substorm injection is likely the energy source of the SAR arc brightening and enhanced poleward motion after 0500 UT, by providing fresh particles into the inner magnetosphere. This explanation assumes that the energy source is due to Coulomb collisions; thus, when the amount of high-energy particles in the equatorial plane interacting with the thermal plasma in the plasmasphere is reduced, the amount of energy transferred to the subauroral ionosphere is reduced, and the consequence is that the T_e decreases and dimmer arcs are observed.The final topic addressed is the shape of the arc observed at Rothera. The sharper poleward edges of the SAR arc at Rothera could be caused by local winter conditions that produce a sharp poleward boundary in the ionospheric trough. During winter conditions, the latitudinal shape of the ionospheric trough boundaries are not uniform, with steeper boundary in the edge connected to the inner ring current (Mendillo & Chacko, 1977), that is, the poleward edge. Using COSMIC (Constellation Observing System for Meteorology, Ionosphere, and Climate) satellite data, He et al. (2011) also showed that ionospheric trough is deeper and more pronounced (i.e., sharper) in the winter hemisphere. This, in turn, means that the excitation in the ionosphere will occur in a steeper region. Evidence for this steeper region can be seen in the DMSP T_e profiles shown in Figure 11. The southern hemisphere data clearly show a sharper variation in the poleward edge, while in the northern hemisphere this sharp variation is not present.

5. Summary

This study has shown that while the overall characteristics of conjugate SAR arcs seem to be similar, there are instances where interhemispheric differences clearly point to asymmetric manifestations of MI coupling. The pair of magnetically conjugate ground-based imagers in Antarctica and North America was used to address these similarities and differences for the first time. The main conclusions we draw from the SAR arc observations made here are as follows:

(i)   The SAR arcs measured simultaneously by both ASIs in the Northern and Southern Hemispheres were magnetically conjugate.

(ii)   The SAR arc at Rothera (local winter) is brighter than the one observed at Millstone Hill (local summer) by a factor of 2-3.

(iii)   The equatorward motion of both arcs is similar, with Rothera's arc moving slightly faster.

(iv)   Brighter and dimmer SAR arcs in both hemispheres, as well as increased and reduced equatorward expansion at both sites, correlate with the increased and reduced magnetospheric forcing.

(v)   The poleward edge of the SAR arc at Rothera is sharper than that at Millstone Hill.

This pair of conjugate point imagers in Antarctica and North America will continue to be used, along with satellite data (e.g., VAP and THEMIS), to address interhemispheric similarities and differences in SAR arcs brightness and shape characteristics. This will lead to quantifying the mechanisms involved in the generation of energy in the equatorial plane that produces SAR arcs at subauroral latitudes under different receptor/seasonal conditions.

References

Barbier, D. (1960). L'arc auroral stable. *Annales Geophysicae*, *16*, 544–549.

Baumgardner, J., Wroten, J., Mendillo, M., Martinis, C., Barbieri, C., Umbriaco, G., et al. (2013). Imaging space weather over Europe. *Space Weather*, *11*, 69–78. https://doi.org/10.1002/swe.20027

Baumgardner, J., Wroten, J., Semeter, J., Kozyra, J., Buonsanto, M., Erickson, P., & Mendillo, M. (2007). A very bright SAR arc: Implications for extreme magnetosphere-ionosphere coupling. *Annales Geophysicae*, *25*. https://doi.org/10.5194/angeo-25-2593-2007

Burke, W. J., Erickson, P. J., Yang, J., Foster, J., Wygant, J., Reeves, G., & Kletzing, C. (2016). O$^+$ ion conic and plasma sheet dynamics observed by Van Allen Probe satellites during the 1 June 2013 magnetic storm. *Journal o f Geophysical Research: Space Physics*, *121*, 4072–4091. https://doi.org/10.1002/2015JA021795

Carman, E. H., Heeran, M. P., & Stevenson, R. W. (1973). Oservation of stable auroral red arcs from Southern Africa. *Planetary and Space Science*, *21*(4), 683–686. https://doi.org/10.1016/0032-0633(73)90079-2

Chamberlain, J. W. (1995). *Physics of the aurora and airglow*. Washington DC: American Geophysicsl Union. https://doi.org/10.1029/SP041

Craven, J. D., Frank, L. A., & Ackerson, K. L. (1982). Global observations of a SAR arc. *Geophysical Research Letters*, *9*(9), 961–964. https://doi.org/10.1029/GL009i009p00961

Fok, M. C., Kozyra, J. U., Nagy, A. F., Rasmussen, C. E., & Khazanov, G. V. (1993). Decay of equatorial ring current ions and associated aeronomical consequences. *Journal of Geophysical Research*, *98*(A11), 19,381–19,393. https://doi.org/10.1029/93JA01848

Fok, M.-C., Kozyra, J. U., Warren, M. F., & Brace, L. H. (1991). Seasonal variations in the subauroral electron temperature enhancement. *Journal of Geophysical Research*, *96*(A6), 9773–9780. https://doi.org/10.1029/91JA00791

Foster, J. C., Buonsanto, M. J., Mendillo, M., Nottingham, D., Rich, F. J., & Denig, W. (1994). Coordinated stable auroral red arc observations: Relationship to plasma convection. *Journal of Geophysical Research*, *99*(A6), 11,429–11,439. https://doi.org/10.1029/93JA03140

Glass, N. W., Wolcott, J. H., Miller, L. W., & Robertson, M. M. (1970). Local time behavior of the alignment and position of a stable auroral red Arc. *Journal of Geophysical Research*, *75*(13). https://doi.org/10.1111/j.1365-2559.1987.tb02625.x

He, M., Liu, L., Wan, W., & Zhao, B. (2011). A study on the nighttime midlatitude ionospheric trough. *Journal of Geophysical Research*, *116*, A05315. https://doi.org/10.1029/2010JA016252

Ichikawa, T., Old, T., & Kim, J. K. (1969). Relationship between a monochromatic auroral arc of 6300 A and a visible aurora. *Journal of Geophysical Research*, *74*(24), 5819–5821.

Kistler, L. M., Mouikis, C. G., Spence, H. E., Menz, A. M., Skoug, R. M., Funsten, H. O., et al. (2016). The source of O$^+$ in the storm time ring current. *Journal of Geophysical Research: Space Physics*, *121*, 5333–5349. https://doi.org/10.1002/2015JA022204

Kozyra, J. U., Nagy, A. F., & Slater, D. W. (1997). High altitude energy source(s) for stable auroral red arcs. *Reviews of Geophysics*, *35*(2), 155–190. https://doi.org/10.1029/96RG03194

LaValle, S. R., & Elliott, D. D. (1972). Observations of SAR arcs from OV1-10. *Journal of Geophysical Research*, *77*(10), 1802–1809. https://doi.org/10.1029/JA077i010p01802

Martinis, C., Baumgardner, J., Mendillo, M., Wroten, J., Coster, A., & Paxton, L. (2015). The night when the auroral and equatorial ionospheres converged. *Journal of Geophysical Research: Space Physics*, *121*, 10,608–10,613. https://doi.org/10.1002/2015JA021555

Martinis, C., Baumgardner, J., Wroten, J., & Mendillo, M. (2017). All-sky-imaging capabilities for ionospheric space weather research using geomagnetic conjugate point observing sites. *Advances in Space Research*, *61*. https://doi.org/10.1016/j.asr.2017.07.021

Martinis, C., Wilson, J., Zablowski, P., Baumgardner, J., Aballay, J. L., Garcia, B., et al. (2013). A new method to estimate cloud cover fraction over El Leoncito Observatory from an all-sky imager designed for upper atmosphere studies. *Publications of the Astronomical Society of the Pacific*, *125*(923).

Mendillo, M., Baumgardner, J., Aarons, J., Foster, J., & Klobuchar, J. (1987). Coordinated optical and radio studies of ionospheric disturbances: Initial results from Millstone Hill. *Annales Geophysicae*, *5A*(6), 543–550.

Mendillo, M., Baumgardner, J., & Wroten, J. (2016). SAR arcs we have seen: Evidence for variability in stable auroral red arcs. *Journal of Geophysical Research: Space Physics*, *121*, 245–262. https://doi.org/10.1002/2015JA021722

Mendillo, M., Baumgardner, J., Wroten, J., Martinis, C., Smith, S., Merenda, K.-D., et al. (2013). Imaging magnetospheric boundaries at ionospheric heights. *Journal of Geophysical Research: Space Physics*, *118*, 7294–7305. https://doi.org/10.1002/2013JA019267

Mendillo, M., & Chacko, C. C. (1977). The baselevel ionospheric trough. *Journal of Geophysical Research*, *82*(32), 5129–5137. https://doi.org/10.1029/JA082i032p05129

Noah, M. A., & Burke, W. J. (2013). Sawtooth-substorm connections: A closer look. *Journal of Geophysical Research: Space Physics*, *118*, 5136–5148. https://doi.org/10.1002/jgra.50440

Reed, E. I., & Blamont, J. E. (1974). Observations of the conjugate SAR arcs of September 28-30, 1967. *Journal of Geophysical Research*, *79*(16).

Rees, M. H., & Roble, R. G. (1975). Observations and theory of the formation of stable auroral red arcs. *Reviews of Geophysics*, *13*, 201.

Richmond, A. (1995). Ionospheric electrodynamics using magnetic apex coordinates. *Journal of Geomagnetism and Geoelectricity*, *47*, 191–212.

Roach, F., & Roach, J. (1963). Stable 6300 Å Auroral arcs in mid-latitudes. *Planetary and Space Science*, *11*, 523–545.

Schaeffer, R. C., & Jacka, F. J. (1971). Stable auroral red arcs observed from Adelaide during 1967-69. *Journal of Atmospheric and Solar-Terrestrial Physics*, *33*, 237–250.

Slater, D., Gurgiolo, C., Kozyra, J. U., Kleckner, E. W., & Winningham, J. D. (1986). A possible SAR arc energization source: Precipitating electrons. *Advances in Space Research*, *6*(3), 133–137.

Slater, D. W., and E. W. Kleckner (1989) Occurrences of stable auroral red arcs detected by the Pacific Northwest Laboratory Photometer Network, 1978-1988, Rep. PNL-7184, Pac. Northwest Lab., Richland, Wash.

Slater, D. W., & Smith, L. L. (1981). Modulation of stable auroral red (SAR) arc occurrence rates. *Journal of Geophysical Research*, *86*(A5), 3669–3673. https://doi.org/10.1029/JA086iA05p03669

Thaller, S. A., Wygant, J. R., Dai, L., Breneman, A. W., Kersten, K., Cattell, C. A., & Bounds, S. R. (2015). Van Allen Probes investigation of the large-scale duskward electric field and its role in ring current formation and plasmasphere erosion in the 1 June 2013 storm. *Journal of Geophysical Research: Space Physics*, *120*, 4531–4543. https://doi.org/10.1002/2014JA020875

Thébault, E., Finlay, C. C., Beggan, C. D., Alken, P., Aubert, J., Barrois, O., et al. (2015). International geomagnetic reference field: The 12th generation. *Earth, Planets and Space*, *67*(1), 1–19. https://doi.org/10.1186/s40623-015-0228-9

Tohmatsu, T., & Roach, F. E. (1962). The morphology of mid-latitude 6300 Angstrom arcs. *Journal of Geophysical Research*, *67*(5), 1817–1821. https://doi.org/10.1029/JZ067i005p01817